RSC Advances

PAPER

View Article Online
View Journal | View Issue

Cite this: *RSC Adv.*, 2020, **10**, 3166

Investigation of the structure and performance of Li[$Li_{0.13}Ni_{0.305}Mn_{0.565}$]$O_2$ Li-rich cathode materials derived from eco-friendly and simple coating techniques†

Xiangnan Li,[abc] Zhaoxia Cao,[abc] Hongyu Dong,[abc] Zhenpu Shi,[abc] Huishuang Zhang,[abc] Junyi Li,[abc] Shuaijia Yang[abc] and Shuting Yang *[abc]

Received 6th November 2019
Accepted 30th December 2019

DOI: 10.1039/c9ra09206d

rsc.li/rsc-advances

Constructing uniform nanoceramic coating layers is a well-known challenge in the field of coating materials. Herein, Al_2O_3-coated Li[$Li_{0.13}Ni_{0.305}Mn_{0.565}$]$O_2$ (LLNM) Li-rich cathode materials are successfully prepared through a dry prilling coating (DPC) method. The structures and electrochemical performances of the Al_2O_3-coated products are systematically examined. Typically, the cycling stability is enhanced and voltage degradation upon cycling is reduced, benefiting from the unique and controllable nano-sized Al_2O_3 coating layer. Moreover, metal ion dissolution is avoided when using the DPC method, which is eco-friendly and suitable for large scale production.

1. Introduction

Lithium ion batteries, which are considered a high-performance and low-cost motive power source, are required for boosting the development and popularity of electric vehicles.[1] Li-rich cathode materials (Li[Ni,Mn]O_2) have attracted extensive research attention due to their high specific capacity and low-cost.[2–5] However, Mn/Ni ion dissolution, structural degradation, polarization effects, side reactions with electrolytes, and electrolyte decomposition at higher potentials result in poor cycling stability at high cut-off voltages.[6–8] In the meantime, non-negligible voltage degradation during cycling and poor rate performance[9–11] severely hinder the performance and potential application of these materials on a large scale. Generally, surface coating,[12,13] interface modification[14–17] and ion-doping[18–26] are widely used and have been proven to be effective strategies to enhance the electrochemical performance of Li-rich cathode materials.[27–32] Among these methods, surface coating with a ceramic layer, such as Al_2O_3, TiO_2 or SiO_2, is a facile and valid technique for improving the cycling stability of Li-rich cathode materials.

Wet chemical synthesis is a common method that is used to form a coating layer on cathode particles. Wang *et al.*[29] reported a freeze-drying method for coating with Al_2O_3, and the long-term cycling performance was enhanced and capacity decay was effectively suppressed in the meantime. Zhang *et al.*[33] reported TiO_2(B)-coated Li[$Li_{0.2}Mn_{0.54}Co_{0.13}Ni_{0.13}$]$O_2$ composites obtained *via* a hydrothermal method, and these showed higher reversible capacity and better cycling stability and rate capabilities. Yang *et al.*[34] synthesized Al_2O_3/SiO_2-coated $Li_{1.2}Mn_{0.54}Ni_{0.13}Co_{0.13}O_2$ *via* a sol–gel method, and the initial coulombic efficiency and capacity retention were improved, while voltage decay was suppressed effectively during charge/discharge cycling. Zheng *et al.*[35] used MgO and TiO_2 to coat $0.5Li_2MnO_3 \cdot 0.5LiNi_{0.5}Co_{0.2}Mn_{0.3}O_2$ cathode materials. The results showed that the surface coating materials could improve the discharge voltage retention, decrease the Li_2CO_3 content on the surface of the materials, and suppress side reactions. However, non-uniform coating and metal-ion leaching were observed during the wet chemical synthesis process. Also, the thickness of the coating layer is usually more than 100 nm, which hinders the diffusion of Li ions. Moreover, water pollution caused by wet chemical reactions is also a signification problem that is concerning.

Physical deposition methods, including atomic layer deposition (ALD) and magnetron sputtering, are considered ideal surface coating techniques. Uniformity and atomic-level control of films can be achieved using these techniques, making them useful for a wide range of applications. Dannehl *et al.*[36] prepared an Al_2O_3-coated $Li_{1.2}Mn_{0.55}Ni_{0.15}Co_{0.1}O_2$ material *via* an ALD method. The results showed that the capacity retention was improved and the initial capacity was increased. Xia *et al.*[37]

[a]School of Physics, School of Chemistry and Chemical Engineering, Henan Normal University, Xinxiang, Henan 453007, China. E-mail: shutingyang@foxmail.com; Tel: +86-373-3323366

[b]National and Local Joint Engineering Laboratory of Motive Power and Key Materials, Xinxiang, Henan 453007, China

[c]Collaborative Innovation Center of Henan Province for Motive Power and Key Materials, Xinxiang, Henan 453007, China

† Electronic supplementary information (ESI) available. See DOI: 10.1039/c9ra09206d

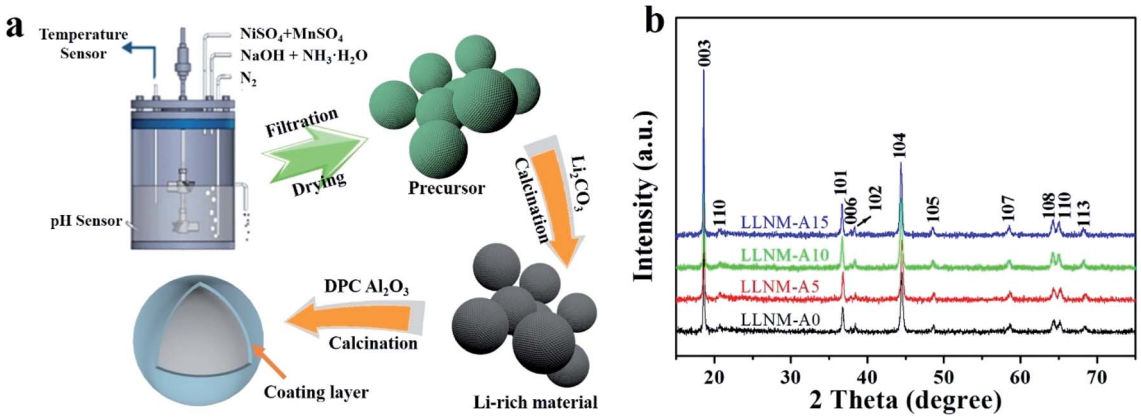

Fig. 1 Graphical illustration of the coating process *via* DPC (a). XRD patterns of the prepared cathode materials (b).

fabricated ZnO-modified $0.3Li_2MnO_3 \cdot 0.7LiNi_{5/21}Co_{5/21}Mn_{11/21}O_2$ cathode materials *via* reactive magnetron sputtering. The experimental data clearly exhibited a much higher initial discharge capacity and coulombic efficiency. Unfortunately, these physical deposition methods rely heavily on sophisticated equipment, and they are not suitable for large-scale industrial production at present.

The dry prilling coating (DPC) method is a facile strategy for material surface modification. As a kind of excellent surface treatment technology, DPC can form uniform coating layers on materials and the thickness of the coating layer can be expediently controlled at the nanoscale. Meanwhile, the procedure is simple and eco-friendly and does not require the use of water, and the cost of production is cheap. The DPC method can satisfactorily meet the demands of whole-scale industrialization, and it has been widely recognized and applied for obtaining powder materials in recent years. Nowadays, it is becoming a prospective strategy for constructing uniform thin films, especially in cases where high reproducibility and excellent conformity are required.

As far as we know, the surface coating of Li-rich cathode materials using DPC has been barely reported previously. This work will validate a novel and simple method for Li-rich cathode materials and provide further understanding of Al_2O_3 coatings obtained with DPC technology. Herein, Li$[Li_{0.13}Ni_{0.305}Mn_{0.565}]O_2$ (LLNM) Li-rich cathode materials with an Al_2O_3 coating are successfully prepared through a dry prilling coating method. The optimized coated samples obtained *via* DPC coating are investigated. The effects of Al_2O_3 coating *via* DPC on the surface morphology before and after cycling, the discharge capacity, the voltage decay, the cycling stability, and Mn/Ni ion dissolution are systematically investigated. The results indicate that appropriate Al_2O_3 coating dosages could effectively improve the electrochemical cycling stability and decrease capacity fading.

2. Experimental section

Detailed experimental information is included in the ESI.†

3. Results and discussion

The simple and efficient DPC strategy includes two processes, mixing and sintering, as shown in Fig. 1a. Fig. 1b shows XRD patterns of samples with different Al_2O_3 coating dosages. The α-$NaFeO_2$ structure with an $R\bar{3}m$ space group, which is ordinarily taken as the signature of a $LiMO_2$ (M = Ni, Mn) phase, is indexed using the diffraction peaks.[24,38] The layered structure can be confirmed *via* the splitting of the (006)/(102) and (108)/(110) peaks.[39] Moreover, the peaks at around 23° originate from superlattice ordering of Li^+ and Mn^{2+} in the layered structure of the transition metal oxide, proving the existence of Li_2MnO_3 ($C2/m$). No other impure phases are detected, which indicates that phase-pure derivatives with layered structures are achieved. Furthermore, lattice parameters of the samples calculated from the XRD patterns are given in Table 1. There are no significant differences in the lattice parameters between the pristine and coated samples, which suggests that this amount of Al_2O_3 coating does not change the crystal structure. The integrated $I(003)/I(104)$ intensity ratio in the XRD patterns of the layered oxides is a measurement of the cation mixing between Li^+ and Ni^{2+}. The $I(003)/I(104)$ values of all the samples are greater than 1.2, illustrating that these materials effectively restrain cation mixing. Also, the $I(003)/I(104)$ values of the coated samples are greater than that of the pristine sample. This suggests that the LLNM structure is more stabilized after Al_2O_3 coating.

Table 1 The calculated lattice parameters of the pristine and coated Li-rich cathode materials

	Lattice parameters			
Sample	a (Å)	c (Å)	c/a	$I(003)/I(004)$
LLNM-A0	2.8579	14.2215	4.9762	1.3271
LLNM-A5	2.8568	14.2187	4.9771	1.4270
LLNM-A10	2.8575	14.2213	4.9768	1.4435
LLNM-A15	2.8580	14.2226	4.9764	1.4255

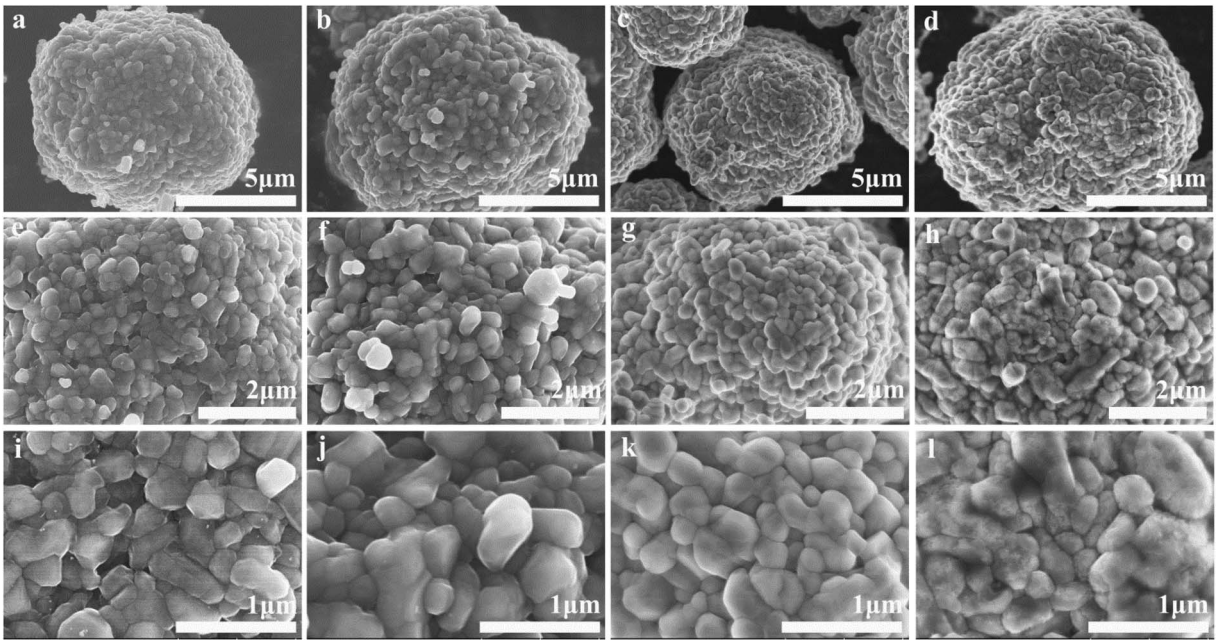

Fig. 2 FESEM images of samples: LLNM-A0 (a, e and i); LLNM-A5 (b, f and j); LLNM-A10 (c, g and k); and LLNM-A15 (d, h and l).

The morphologies of Al_2O_3, a pristine sample, and the series of Al_2O_3-coated samples were confirmed *via* FESEM (Fig. S1† and 2). Both the pristine and coated materials contain fine and uniform particles ranging from 8 to 12 μm in diameter. The surfaces of the pristine spherical particles are smooth, with slight extensions resulting from primary particles (Fig. 2a, e and i); this is very different from the coated samples. The surfaces of LLNM samples coated with nanoscale Al_2O_3 particles *via* DPC are fuzzy. In particular, with an increase in the Al_2O_3 content, the roughness of the coated samples increased significantly. When the Al_2O_3 content is increased to 1.5 wt%, the LLNM sample is totally covered and the surface is rougher than the other Al_2O_3-coated samples, which may imply that the amount of Al_2O_3 exceeds requirements.

Similarly, SEM images and elemental mapping of an LLNM-A10 sample are also provided (Fig. S2†). Mn, Ni and trace Al

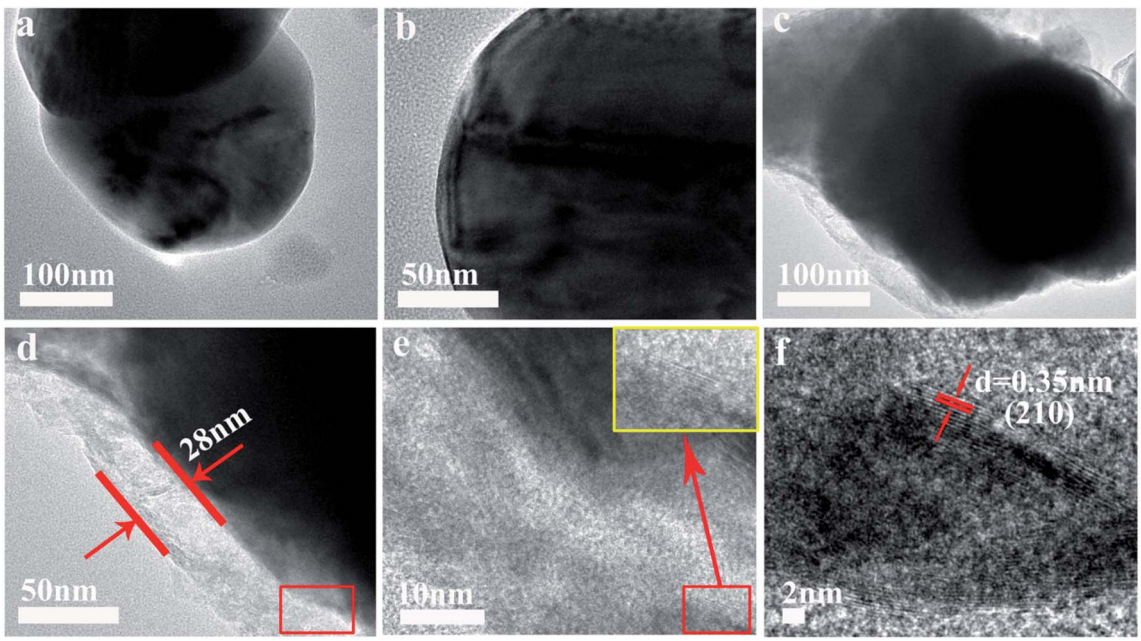

Fig. 3 TEM images (a and c) and HRTEM (b and d) images of LLNM-A0 and LLNM-A10, respectively. (e) An enlargement of the red rectangle area in (d). (f) An enlargement of the red rectangle area in (e).

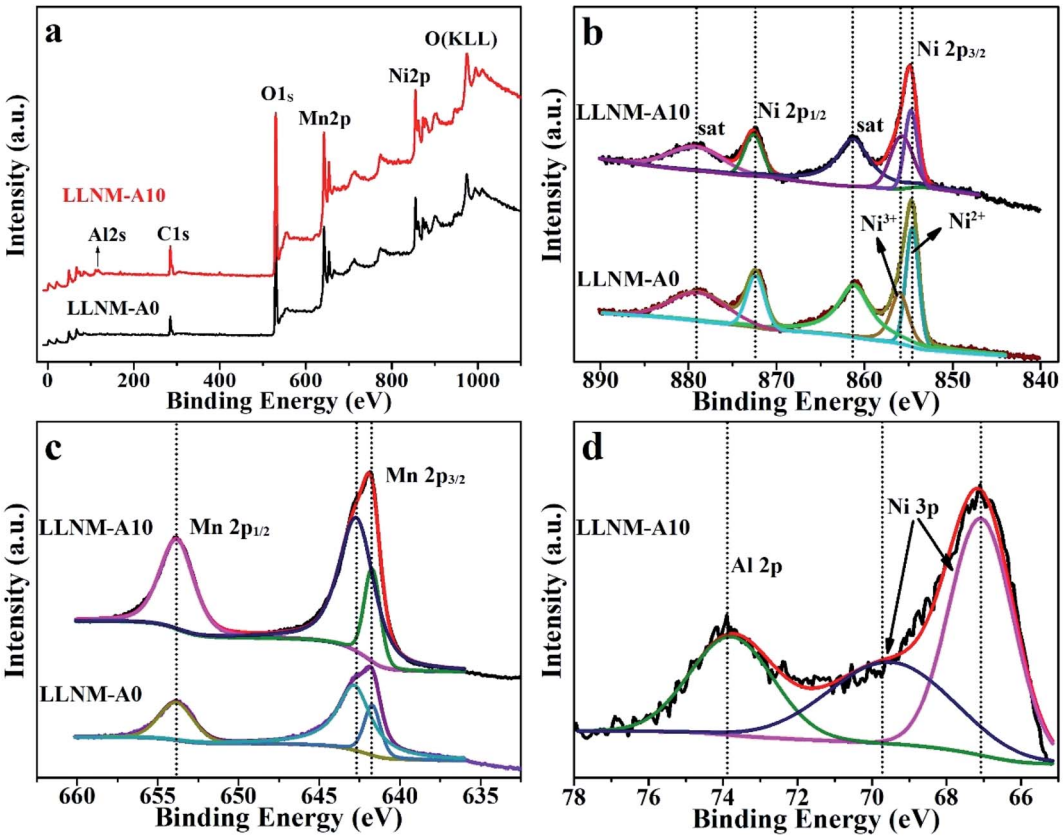

Fig. 4 XPS survey spectra (a), Ni 2p spectra (b), and Mn 2p spectra (c) of LLNM-A0 and LLNM-A10 and the Al 2p spectrum (d) of LLNM-A10.

elements exist on the particles of LLNM. The uniform distribution of Mn, Ni and Al clearly illustrates that their distribution is similar to what is seen in Fig. S2a.† This also verifies the homogeneous nature of the LLNM-A10 particles. Combining the elemental distribution mapping and SEM images, it can be proved that Al_2O_3 successfully coated the obtained materials.

Fig. 3 shows HRTEM images of LLNM-A0 and LLNM-A10. The images clearly show the bulk particles of the pristine and coated samples. The pristine material LLNM-A0 displays smooth boundaries without any coating layer on the surface (Fig. 3a and b). For the coated sample of LLNM-A10 (Fig. 3c), some Al_2O_3 nanoparticles are distributed on the LLNM material; the thickness of the coating layer is 28 nm (Fig. 3d), which illustrates that a coating layer has been obtained. Fig. 3e and f further demonstrate the presence of Al_2O_3 (Fig. 3e and f show partial enlargements of Fig. 3d and e). As displayed in Fig. 3f, the interplanar spacing of 0.35 nm corresponds to the (210) plane of Al_2O_3.[28] A uniform modification layer is helpful to suppress the dissolution of transition metal ions and maintain structural stability during the charge–discharge process. The Al_2O_3 coating layer is further probed *via* Ni, Mn, O, and Al elemental mapping using HRTEM (Fig. S3†). The Al elements are uniformly distributed in the LLNM-A10 sample, which shows that Al_2O_3 has coated the obtained materials successfully.

X-ray photoelectron spectroscopy (XPS) analysis was performed in order to confirm the oxidation states of Ni, Mn and Al. The C 1s peak (284.4 eV) is used to calibrate the binding energy (BE). The elements Ni, Mn and Al in LLNM-A0 and LLNM-A10 are detected in the survey spectrum, as shown in Fig. 4a. The XPS spectra of Ni 2p, Mn 2p and Al 2p species are further illustrated in Fig. 4b–d, respectively. In the Ni 2p spectra, the peak located at 872.3 eV with a satellite peak at 879.1 eV is attributed to Ni $2p_{1/2}$. The Ni $2p_{3/2}$ peaks in the spectra located at 854.1 and 855.4 eV, with a satellite peak at 861.0 eV, are assigned to Ni^{2+} and Ni^{3+}, respectively. Ni exists as a mixture of +2 and +3 valence states.[40,41] The Mn $2p_{1/2}$ and Mn $2p_{3/2}$ XPS peaks are located at about 653.9 eV and 642.1 eV, respectively, which demonstrates that the main valence state of Mn is +4.[20,40] The peak at 73.8 eV in the Al 2p spectrum is assigned to Al^{3+} in Al_2O_3.[42] Moreover, the Al 2p spectrum of the DPC derived sample is in accordance with previously reported results from Al_2O_3 coatings.[28] The XPS results indicate that Al_2O_3 is successfully coated on the surface of LLNM.

Fig. 5 and S4–S8 (ESI†) present the cycling performance and charge–discharge curves of the pristine and coated materials at 0.1C (activated for an initial three cycles, 1C = 300 mA g^{-1}) and 1C at room temperature. The LLNM-A0 sample manifests excellent discharge capacities (254.4 mA h g^{-1} and 186.5 mA h g^{-1} for the first cycle at 0.1C and 1C, respectively). Al_2O_3 is inactive during the charge–discharge process, which results in distinct initial polarization and specific capacity loss being shown by the coated samples. This can probably be attributed to increases in the contact resistance and charge

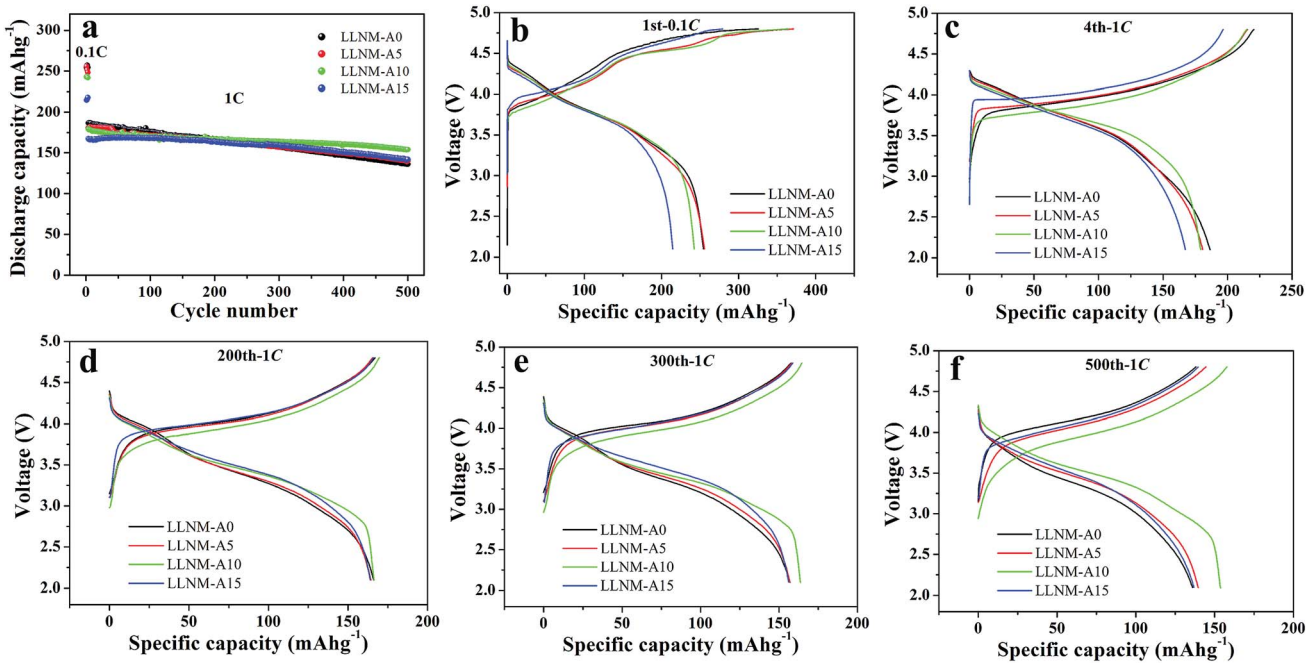

Fig. 5 The long-term cycling performance (a), and charge–discharge curves after the 1st (b), 4th (c), 200th (d), 300th (e) and 500th (f) cycle at 0.1C and 1C of pristine and coated samples.

transfer resistance. However, the Al_2O_3-coated samples present more stable long-term cycling performance than the pristine sample. As the cycling goes on, the LLNM-A0 sample capacity retention is approximately level with the LLNM-A10 sample after 200 cycles at 1C. And after 500 cycles, LLNM-A10 displays a higher capacity retention ratio (85.87%) than the pristine sample (72.92%). Appropriate coating with Al_2O_3 could effectively decrease polarization, which is beneficial for decreasing capacity fading and improving cycling stability performance.

To better describe and understand the effects of Al_2O_3 coating *via* DPC on the electrochemical performance, Fig. 6 shows the discharge behaviors of pristine and Al_2O_3-coated samples at 1C. Obviously, there are remarkable differences between the discharge voltage plateaus of LLNM-A0 and LLNM-A10. The voltage decay of the discharge plateaus is suppressed by the Al_2O_3 coating layer. Upon cycling, the discharge capacity of LLNM-A0 (Fig. 6a) decreases at a faster rate than LLNM-A10 (Fig. 6b). It can be found that the LLNM-A0 sample undergoes rapid voltage decay (0.31 V) from the 4th to the 500th cycle at 1C, which is much higher than that undergone by LLNM-A10 (0.22 V). Benefiting from the effective coating technology and synergistic effects arising from the Al_2O_3 coating thickness, using the DPC method to coat LLNM could restrain discharge voltage fading upon cycling. As illustrated in Fig. 6, the Al_2O_3 coating layer plays a central role in slowing voltage fading polarization. These results indicate that this coating strategy may suppress interfacial reactions between the cathode material and the electrolyte, reducing interfacial resistance.

To demonstrate the suppression of transition metal ion dissolution by the Al_2O_3 coating layer on the LLNM material, ICP analyses of electrodes were carried out after 500 cycles. Fig. 6c illustrates that transition metal ion dissolution levels in the LLNM-A10 sample were obviously less than in the LLNM-A0 sample. This is a result of the appropriate Al_2O_3 coating

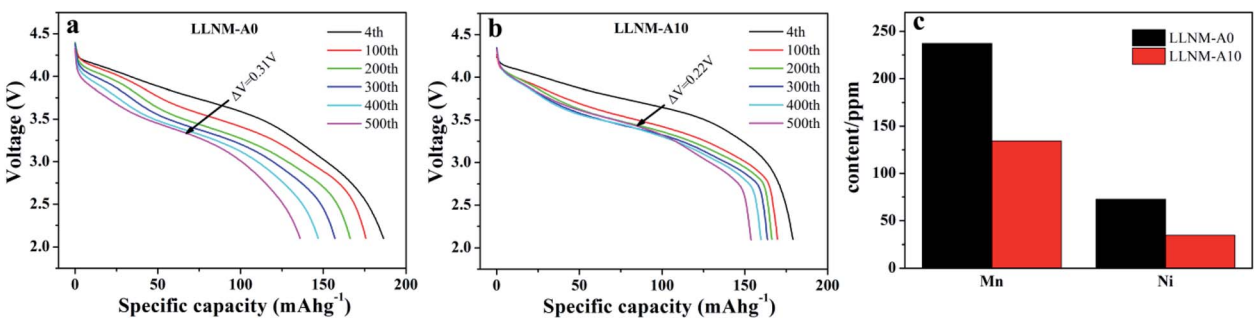

Fig. 6 Discharge curves of LLNM-A0 (a) and LLNM-A10 (b) at 25 °C at 1C. The dissolution of transition metal ions from LLNM-A0 and LLNM-A10 samples (c).

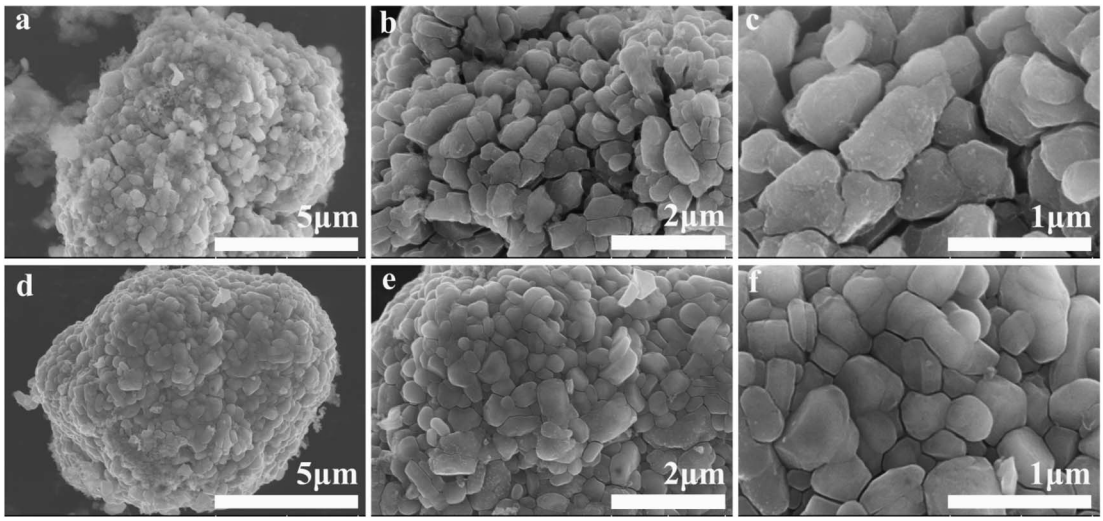

Fig. 7 FESEM images of LLNM-A0 (a–c) and LLNM-A10 (d–f) samples after 500 cycles.

strategy. This indicates that Al_2O_3 coating *via* DPC technology could stabilize the framework and decrease Mn/Ni ion dissolution from the LLNM cathode material, improving the structural stability over numerous battery cycles.

FESEM and EDS analysis of typical pristine and Al_2O_3-coated samples after 500 cycles was carried out in order to further figure out how Al_2O_3 coating *via* DPC technology affected the cycling stability. LLNM-A0 and LLNM-A10 electrode samples were soaked and washed after 500 charge–discharge cycles before observations were made. As shown in Fig. 7a–c, the images manifest that a number of cracks appeared and the structure deteriorated in the case of LLNM-A0. By contrast, these phenomena are not found in the case of LLNM-A10. Also, the Al_2O_3 coating layer maintains its morphological and structural

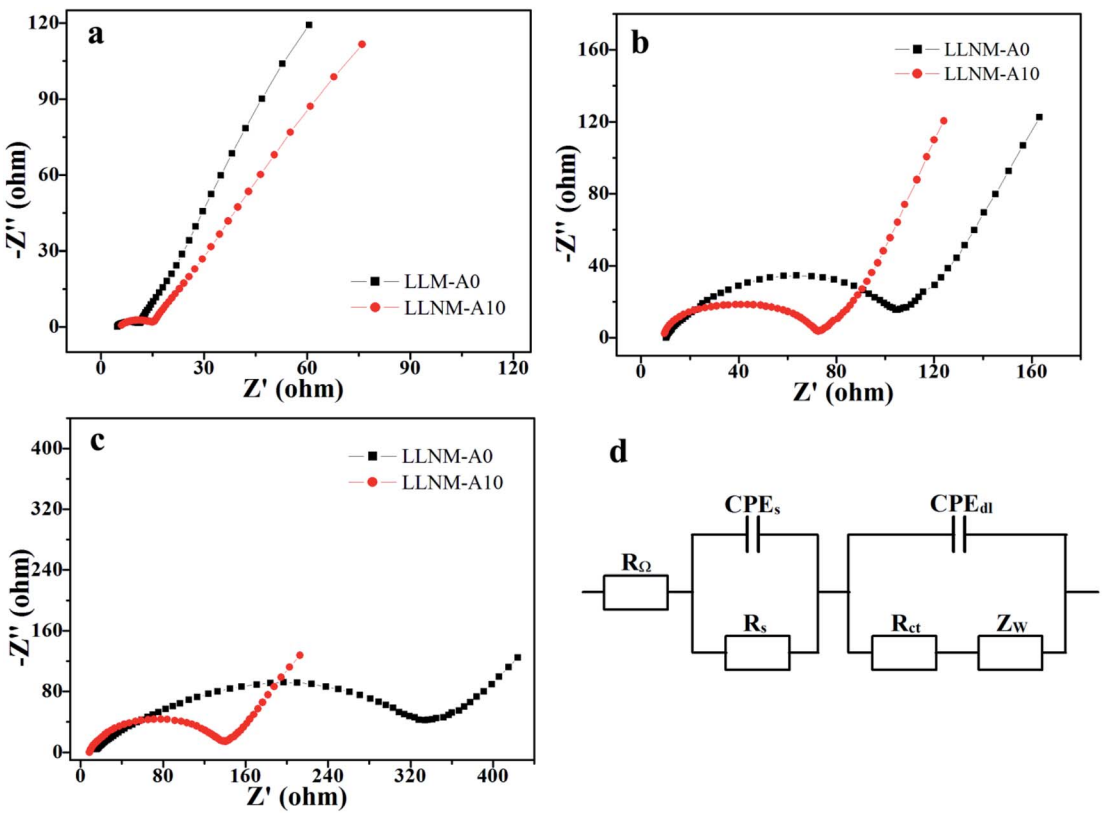

Fig. 8 AC impedance spectra from LLNM-A0 and LLNM-A10 samples before cycling (a), after 300 cycles (b), and after 500 cycles (c), and the equivalent circuit diagram (d).

completeness, indicating reduced volume change (Fig. 7d–f). The homogeneous distribution of Mn, Ni and Al elements on the surface of LLNM, as shown in the element mapping in Fig. S9,† reveals that the coating layer remains nearly intact after 500 cycles, thus effectively protecting LLNM from HF attack.[43]

Electrochemical impedance spectra (EIS) from LLNM-A0 and LLNM-A10 before and after different numbers of cycles and the corresponding equivalent circuit diagram are shown in Fig. 8. The Nyquist plots are formed from a semicircle in the high frequency region and an oblique line in the low frequency region. The large intercept with the real axis demonstrates the large ohmic resistance of the cell.[21] In addition, the depressed semicircle is caused by reaction processes at the electrolyte/electrode interface.[7] The oblique line in the lower frequency range is attributed to Warburg impedance, which was associated with lithium ion diffusion through the cathode electrode.

The LLNM-A0 sample manifests excellent R_{ct} and Z_W values before cycling. However, as the number of cycles increases, it is obviously seen that the R_{ct} and Z_W values of LLNM-A0 are visibly increased compared with LLNM-A10. It is indicated that this is consistent with the battery discharge capacities of LLNM-A0 and LLNM-A10. Furthermore, the R_{ct} and Z_W values of LLNM-A0 and LLNM-A10 are increased, but the R_Ω values remain approximately similar. It can be inferred that the use of the same conductive agent is the primary cause. The results indicate that the coating dosage maintains a compromise between impedance and polarization: the surface Al_2O_3 coating slows down the Li mobility in LLNM-A10, while it is beneficial for improving the structural stability of the active material and decreasing polarization.

4. Conclusions

In this work, an Al_2O_3 thin coating layer on LLNM cathode materials has been successfully obtained through DPC technology. Samples with different Al_2O_3 coating dosages obtained *via* a DPC strategy are investigated. An optimized Al_2O_3 coating layer thickness is beneficial for enhancing the cycling stability of the LLNM cathode materials. At 25 °C and 1C, LLNM-A10 displays a higher capacity retention ratio (85.87%) than a pristine sample (72.92%) after 500 cycles. Meanwhile, the LLNM-A10 sample effectively restrains voltage degradation to about 0.22 V from the 4th to the 500th cycle at 1C. Typically, LLNM-A10 exhibits better material structural stability and cycling performance in batteries compared to the pristine sample. The excellent structural properties and cycling stability can be attributed to the Al_2O_3 coating layer, which can effectively prevent direct contact between the electrolyte and active material, decrease polarization, and suppress the dissolution of transition metal ions upon cycling. Also, the coating layer will influence the initial discharge efficiency and electrochemical impedance. This study intends to illustrate the characteristics of Al_2O_3 coating methods and provide some enlightenment regarding further scientific research into lithium ion battery cathode materials and their industrial application. Meanwhile, we hope that these study results can offer and assist the choice of this simple and eco-friendly Al_2O_3 coating technology for LLNM cathode materials.

Conflicts of interest

There are no conflicts to declare.

Acknowledgements

This work was financially supported by the Key Project of Science and Technology of Henan Educational Department (No. 20B430009).

References

1 H. Y. Yue, J. X. Li, Q. X. Wang, C. B. Li, Q. H. Li, X. N. Li, H. S. Zhang and S. T. Yang, Sandwich-Like Poly(Propylene Carbonate)-Based Electrolyte for Ambient-Temperature Solid-State Lithium Ion Batteries, *ACS Sustainable Chem. Eng.*, 2018, **6**(1), 268–274.

2 M. M. Thackeray, C. S. Johnson, J. T. Vaughey, N. Li and S. A. Hackney, Advances in manganese-oxide 'composite' electrodes for lithium-ion batteries, *J. Mater. Chem.*, 2005, **15**(23), 2257–2267.

3 M. M. Thackeray, S.-H. Kang, C. S. Johnson, J. T. Vaughey, R. Benedek and S. A. Hackney, Li_2MnO_3-stabilized $LiMO_2$ (M = Mn, Ni, Co) electrodes for lithium-ion batteries, *J. Mater. Chem.*, 2007, **17**(30), 3112–3125.

4 C. S. Johnson, J.-S. Kim, A. J. Kropf, A. J. Kahaian, J. T. Vaughey and M. M. Thackeray, The role of Li_2MO_2 structures (M = metal ion) in the electrochemistry of $(x)LiMn_{0.5}Ni_{0.5}O_2 \cdot (1-x)Li_2TiO_3$ electrodes for lithium-ion batteries, *Electrochem. Commun.*, 2002, **4**, 492–498.

5 C. S. Johnson, J.-S. Kim, C. Lfief, N. Li, J. T. Vaughey and M. M. Thackeray, The significance of the Li_2MnO_3 component in 'composite' $xLi_2MnO_3 \cdot (1-x)LiMn_{0.5}Ni_{0.5}O_2$ electrodes, *Electrochem. Commun.*, 2004, **6**(10), 1085–1091.

6 J. Liu, Q. Y. Wang, B. Reeja-Jayan and A. Manthiam, Carbon-coated high capacity layered $Li[Li_{0.2}Mn_{0.54}Ni_{0.13}Co_{0.13}]O_2$ cathodes, *Electrochem. Commun.*, 2010, **12**(6), 750–753.

7 J. M. Zheng, X. B. Wu and Y. Yang, A comparison of preparation method on the electrochemical performance of cathode material $Li[Li_{0.2}Mn_{0.54}Ni_{0.13}Co_{0.13}]O_2$ for lithium ion battery, *Electrochim. Acta*, 2011, **56**(8), 3071–3078.

8 T. R. Penki, P. K. Nayak, E. Levi, J. Grinblat, Y. Elias, S. Luski, B. Markovsky and D. Aurbach, Reaching Highly Stable Specific Capacity with Integrated $0.6Li_2MnO_3$:$0.4LiNi_{0.6}Co_{0.2}Mn_{0.2}O_2$ Cathode Materials, *ChemElectroChem*, 2018, **5**(8), 1137–1146.

9 E.-S. Lee and A. Manthiram, Smart design of lithium-rich layered oxide cathode compositions with suppressed voltage decay, *J. Mater. Chem. A*, 2014, **2**(11), 3932–3939.

10 E. M. Erickson, F. Schipper, R. Y. Tian, J.-Y. Shin, C. Erk, F. F. Chesneau, J. K. Lampert, B. Markovsky and D. Aurbach, Enhanced capacity and lower mean charge voltage of Li-rich cathodes for lithium ion batteries

resulting from low-temperature electrochemical activation, *RSC Adv.*, 2017, **7**(12), 7116–7121.

11 S. Chen, L. Chen, Y. T. Li, Y. F. Su, Y. Lu, L. Y. Bao, J. Wang, M. Wang and F. Wu, Synergistic Effects of Stabilizing the Surface Structure and Lowering the Interface Resistance in Improving the Low-Temperature Performances of Layered Lithium-Rich Materials, *ACS Appl. Mater. Interfaces*, 2017, **9**(10), 8641–8648.

12 C.-C. Wang, J.-W. Lin, Y.-H. Yu, K.-H. Lai, K.-F. Chiu and C.-C. Kei, Electrochemical and Structural Investigation on Ultrathin ALD ZnO and TiO_2 Coated Lithium-Rich Layered Oxide Cathodes, *ACS Sustainable Chem. Eng.*, 2018, **6**(12), 16941–16950.

13 X. H. Zhang, R. Z. Yu, Y. Huang, X. Y. Wang, Y. Wang, B. Wu, Z. S. Liu and J. C. Chen, The influences of surface coating layers on the properties of layered/spinel heterostructured Li-rich cathode material, *ACS Sustainable Chem. Eng.*, 2018, **6**(10), 12969–12979.

14 F. X. Ding, J. L. Li, F. H. Deng, G. F. Xu, Y. Y. Liu, K. Yang and F. Y. Kang, Surface Heterostructure Induced by $PrPO_4$-modifying in $Li_{1.2}[Mn_{0.54}Ni_{0.13}Co_{0.13}]O_2$ cathode material for high performance lithium ion batteries with Mitigating Voltage Decay, *ACS Appl. Mater. Interfaces*, 2017, **9**(33), 27936–27945.

15 S. Q. Yang, P. B. Wang, H. X. Wei, L. B. Tang, X. H. Zhang, Z. J. He, Y. J. Li, H. Tong and J. C. Zheng, $Li_4V_2Mn(PO_4)_4$-stablized $Li[Li_{0.2}Mn_{0.54}Ni_{0.13}Co_{0.13}]O_2$ cathode materials for lithium ion batteries, *Nano Energy*, 2019, **63**, 103889–103899.

16 Y. J. Zhao, X. S. Hu, C. W. Ji, Y. c. Sun, Y. Wang, Z. K. Zhao and Z. Lv, Surface Basicity Induced RuO_2 Modification on Nanosized Li-Rich Cathode $Li_{1.26}Fe_{0.22}Mn_{0.52}O_2$ with Superior Electrochemical Performance, *J. Electrochem. Soc.*, 2016, **163**(9), 2040–2046.

17 X. N. Li, Z. X. Cao, H. Y. Yue, Q. X. Wang, H. S. Zhang and S.-T. Yang, Tuning Primary Particle Growth of $Li_{1.2}Ni_{0.2}Mn_{0.6}O_2$ by Nd-Modification for Improving the Electrochemical Performance of Lithium Ion Batteries, *ACS Sustainable Chem. Eng.*, 2019, **7**(6), 5946–5952.

18 G. R. Chen, J. An, Y. M. Meng, C. Z. Yuan, B. Matthews, F. Dou, L. Y. Shi, Y. F. Zhou, P. G. Song, G. Wu and D. S. Zhang, Cation and Anion Co-doping Synergy to Improve Structural Stability of Li- and Mn-rich Layered Cathode Materials for Lithium-ion Batteries, *Nano Energy*, 2019, **57**, 157–165.

19 J. An, L. Y. Shi, G. R. Chen, M. S. Li, H. J. Liu, S. Yuan, S. M. Chen and D. S. Zhang, Insights into the stable layered structure of a Li-rich cathode material for lithium-ion batteries, *J. Mater. Chem. A*, 2017, **5**, 19738–19744.

20 Y. J. Zhao, M. H. Xia, X. S. Hu, Z. K. Zhao, Y. Wang and Z. Lv, Effects of Sn doping on the structural and electrochemical properties of $Li_{1.2}Ni_{0.2}Mn_{0.8}O_2$ Li-rich cathode materials, *Electrochim. Acta*, 2015, **174**, 1167–1174.

21 L. L. Xue, Y. J. Li, B. Xu, Y. X. Chen, G. L. Cao, J. G. Li, S. Y. Deng, Y. J. Chen and J. Chen, Effect of Mo doping on the structure and electrochemical performances of $LiNi_{0.6}Co_{0.2}Mn_{0.2}O_2$ cathode material at high cut-off voltage, *J. Alloys Compd.*, 2018, **748**, 561–568.

22 X. Hu, H. J. Guo, W. J. Peng, Z. X. Wang, X. H. Li and Q. Y. Hu, Effects of Nb doping on the performance of $0.5Li_2MnO_3 \cdot 0.5LiNi_{1/3}Co_{1/3}Mn_{1/3}O_2$ cathode material for lithium-ion batteries, *J. Electroanal. Chem.*, 2018, **822**, 57–65.

23 M. Eilers-Rethwisch, S. Hildebrand, M. Evertz, M. Ibing, T. Dagger, M. Winter and F. M. Schappacher, Comparative study of Sn-doped $Li[Ni_{0.6}Mn_{0.2}Co_{0.2-x}Sn_x]O_2$ cathode active materials ($x = 0$ – 0.5) for lithium ion batteries regarding electrochemical performance and structural stability, *J. Power Sources*, 2018, **397**, 68–78.

24 H. Chen, Q. Y. Hu, Z. M. Huang, Z. J. He, Z. X. Wang, H. J. Guo and X. H. Li, Synthesis and electrochemical study of Zr-doped $Li[Li_{0.2}Mn_{0.54}Ni_{0.13}Co_{0.13}]O_2$ as cathode material for Li-ion battery, *Ceram. Int.*, 2016, **42**(1), 263–269.

25 L. Li, B. H. Song, Y. L. Chang, H. Xia, J. R. Yang, K. S. Lee and L. Lu, Retarded phase transition by fluorine doping in Li-rich layered $Li_{1.2}Mn_{0.54}Ni_{0.13}Co_{0.13}O_2$ cathode material, *J. Power Sources*, 2015, **283**, 162–170.

26 Z. Zheng, X.-D. Guo, Y.-J. Zhong, W.-B. Hua, C.-H. Shen, S.-L. Chou and X.-S. Yang, Host Structural Stabilization of $Li_{1.232}Mn_{0.615}Ni_{0.154}O_2$ through K-Doping Attempt: toward Superior Electrochemical Performances, *Electrochim. Acta*, 2016, **188**, 336–343.

27 Z. J. He, Z. X. Wang, H. J. Guo, X. H. Li, X. W. Wu, P. Yue and J. X. Wang, A simple method of preparing graphene-coated $Li[Li_{0.2}Mn_{0.54}Ni_{0.13}Co_{0.13}]O_2$ for lithium-ion batteries, *Mater. Lett.*, 2013, **91**, 261–264.

28 X. F. Wen, K. Liang, L. Y. Tian, K. Y. Shi and J. S. Zheng, Al_2O_3 coating on $Li_{1.256}Ni_{0.198}Co_{0.082}Mn_{0.689}O_{2.25}$ with spinel-structure interface layer for superior performance lithium ion batteries, *Electrochim. Acta*, 2018, **260**, 549–556.

29 J. P. Wang, C. Y. Du, C. Q. Yan, X. S. He, B. Song, G. P. Yin, P. J. Zuo and X. Q. Cheng, Al_2O_3 Coated Concentration-Gradient $Li[Ni_{0.73}Co_{0.12}Mn_{0.15}]O_2$ Cathode Material by Freeze Drying for Long-Life Lithium Ion Batteries, *Electrochim. Acta*, 2015, **174**, 1185–1191.

30 X. P. Zhang, S. W. Sun, Q. Wu, N. Wan, D. Pan and Y. Bai, Improved electrochemical and thermal performances of layered $Li[Li_{0.2}Ni_{0.17}Co_{0.07}Mn_{0.56}]O_2$ via Li_2ZrO_3 surface modification, *J. Power Sources*, 2015, **282**, 378–384.

31 J.-H. Zhang, W.-J. Wang, B. Zhang, D.-B. Zhang and J.-C. Song, Upper bound solution for required supporting pressure applied on a deep shield tunnel face under different groundwater levels, *Geotech. Geol. Eng.*, 2019, **37**, 491.

32 Y. W. Chen, X. C. Wang, J. J. Zhan, B. Y. Chen, J. M. Xu, S. Zhang and L. W. Zhang, Al_2O_3-coated $Li_{1.2}Mn_{0.54}Ni_{0.13}Co_{0.13}O_2$ nanotubes as cathode materials for high-performance lithiumion batteries, *RSC Adv.*, 2019, **9**, 2172–2179.

33 Y. P. Gan, Y. S. Wang, J. F. Han, L. Y. Zhang, W. Sun, Y. Xia, H. Huang, J. Zhang, C. Liang and W. K. Zhang, Synthesis and electrochemical performance of nano TiO_2(B)-coated $Li[Li_{0.2}Mn_{0.54}Co_{0.13}Ni_{0.13}]O_2$ cathode materials for lithium-ion batteries, *New J. Chem.*, 2017, **41**, 12962–12968.

34 W. X. Zhang, Y. T. Liu, J. L. Wu, H. X. Shao and Y. F. Yang, Surface modification of $Li_{1.2}Mn_{0.54}Ni_{0.13}Co_{0.13}O_2$ cathode

material with Al_2O_3/SiO_2 composite for lithium-ion batteries, *J. Electrochem. Soc.*, 2019, **166**(6), 863–872.

35 B. Xiao, P. B. Wang, Z.-J. He, Z. Yang, L. B. Tang, C. S. An and J. C. Zheng, Effect of MgO and TiO_2 coating on the electrochemical performance of Li-rich cathode materials for lithium-ion batteries, *Energy Technol.*, 2019, 7(8), 1800829–1800838.

36 N. Dannehl, S. O. Steinmuller, D. V. Szabo, M. Pein, F. Sigel, L. Esmezjan, U. Hasenkox, B. Schwarz, S. Indris and H. Ehrenberg, High-resolution surface analysis on aluminum oxide-coated $Li_{1.2}$ $Mn_{0.55}Ni_{0.15}Co_{0.1}O_2$ with improved capacity retention, *ACS Appl. Mater. Interfaces*, 2018, **10**(49), 43131–43143.

37 B. Qiu, J. Wang, Y. G. Xia, Z. Wei, S. J. Han and Z. P. Liu, Enhanced electrochemical performance with surface coating by reactive magnetron sputtering on lithium-rich layered oxide electrodes, *ACS Appl. Mater. Interfaces*, 2014, **6**(12), 9185–9193.

38 C. X. Zhou, P. B. Wang, B. Zhang, J. C. Zheng, Y. Y. Zhou, C. H. Huang and X. M. Xi, Suppressing the voltage fading of $Li[Li_{0.20}Ni_{0.133}Co_{0.133}Mn_{0.534}]O_2$ cathode material via Al_2O_3 coating for Li-ion batteries, *J. Electrochem. Soc.*, 2018, **165**(9), 1648–1655.

39 A. Rougier, P. Gravereau and C. Delmas, Optimization of the Composition of the $Li_{1-z}Ni_{1+z}O_2$ Electrode Materials: Structural, Magnetic, and Electrochemical Studies, *J. Electrochem. Soc.*, 1996, **143**(4), 1168–1175.

40 H. Wang, W. Ge, W. Li, F. Wang, W. J. Liu, M.-Z. Qu and G. C. Peng, Facile fabrication of ethoxy-functional polysiloxane wrapped $LiNi_{0.6}Co_{0.2}Mn_{0.2}O_2$ cathode with improved cycling performance for rechargeable Li-ion battery, *ACS Appl. Mater. Interfaces*, 2016, **8**(28), 18439–18449.

41 D. T. Nguyen, J. Kang, K. M. Nam, Y. Paik and S. W. Song, Understanding interfacial chemistry and stability for performance improvement and fade of high-energy Li-ion battery of $LiNi_{0.5}Co_{0.2}Mn_{0.3}O_2$//silicon–graphite, *J. Power Sources*, 2016, **303**, 150–158.

42 C. D. Wagner, D. E. Passoja, H. F. Hillery, T. G. Kinisky, H. A. Six, W. T. Jansen and J. A. Taylor, Auger and photoelectron line energy relationships in aluminum–oxygen and silicon–oxygen compounds, *J. Vac. Sci. Technol.*, 1982, **21**(4), 933–944.

43 Z. X. Cao, Y. L. Li, M. J. Shi, G. S. Zhu, R. R. Zhang, X. N. Li, H. Y. Yue and S. T. Yang, Improvement of the cycling performance and thermal stability of Lithium-ion batteries by coating cathode materials with Al_2O_3 nano layer, *J. Electrochem. Soc.*, 2017, **164**(2), 475–481.

